Title

Hydroxypyridinone-based stabilization of Np(IV) enabling efficient U/Np/Pu separations in the Adapted PUREX process

Authors

Wang, Yufei
Zhang, Zhicheng
Abergel, Rebecca J

Publication Date

2021-03-01

DOI

10.1016/j.seppur.2020.118178

Peer reviewed

Hydroxypyridinone-based stabilization of Np(IV) enabling efficient U/Np/Pu separations in the Adapted PUREX process

Yufei Wang[†,‡], Zhicheng Zhang[‡], Rebecca J. Abergel[†,‡,*]

[†] *Department of Nuclear Engineering, University of California, Berkeley, California 94720, USA.*

[‡] *Chemical Sciences Division, Lawrence Berkeley National Laboratory, Berkeley, California 94720, USA.*

**Corresponding author: abergel@berkeley.edu*

Keywords: Separation; Hydroxypyridinone; Neptunium; PUREX; Reduction.

Highlights

- A water-soluble hydroxypyridinone-based ligand was evaluated for U/Np/Pu separations in the context of an adapted PUREX process.
- Model compound 3,4,3-LI(1,2-HOPO) was demonstrated to stabilize Np in the +4 oxidation state by spectrophotometric and electrochemical methods.
- Under very high acidities, introduction of this aqueous chelating agent enhanced separations by liquid-liquid extraction among the actinide trio, UO_2^{2+}, NpO_2^{+}, and Pu^{4+}.

Abstract: The classical process to recover uranium (U) and plutonium (Pu) from used nuclear fuel using tributyl phosphate (TBP), namely the Plutonium Uranium Redox EXtraction (PUREX) process, is complicated by the persistent presence of neptunium (Np) and thus requires extra purification steps. The concept of Adapted PUREX seeks to achieve Np recovery by adjusting the valence of the metal more effectively, thereby controlling its behavior more precisely. This study introduces the use of an aqueous hydroxypyridinone chelator, 3,4,3-LI(1,2-HOPO) (abbreviated as HOPO), to dictate the behavior of Np for recovery and meanwhile simplify cumbersome reprocessing steps. The interactions between Np and HOPO were probed mechanistically by way of absorption spectrophotometry, in conjunction with cyclic voltammetry. UV-Vis-NIR spectra illustrated the reduction of NpO_2^{2+} to Np^{4+}, with a fast reaction rate. Cyclic voltammetry revealed quasi-reversible processes between the oxidized and reduced forms of the ligand and its Np complexes. The corresponding heterogeneous rate constants (k_0) were estimated from the peak-to-peak separation potentials (ΔE_p), at ~4 – 35 μm/s for both HOPO and NpHOPO, with scan rates of 0.01 – 0.4 V/s. Meanwhile, the electromotive force (E_{MF}) as well as the change of Gibbs free energy (ΔG) were assessed from the half-wave potential ($E_{1/2}$), demonstrating the completeness of NpO_2^{2+} reduction to Np^{4+} by HOPO. The cumulative formation constant of the resulting NpHOPO complex ($\log\beta_{101}$) was determined by metal competition titration to be 42.0 ± 0.6, corroborating the extraordinarily high affinity of HOPO to tetravalent metal ions. The prowess of valence control by HOPO and the high stability of the formed complex resulted in enhanced separations of Np from U and of Pu from U, with a maximum separation factor of ~7000 for both, nearly 90- and 10300-fold higher, respectively, than the values obtained using conventional PUREX formulae.

Introduction

Used nuclear fuel (UNF) contains an appreciable amount of ^{237}Np, which is generated by (n, γ) reactions of ^{235}U and by (n, 2n) reactions of ^{238}U, followed by β^- decay of ^{237}U [1]. As the longest-lived member ($t_{1/2} = 2.14\times10^6$ yr) of the 4n + 1 radioactive decay series, ^{237}Np is an important and problematic long-term radiotoxic constituent of high level liquid waste (HLLW). A commonly-accepted fate of Np is to be routed to HLLW for vitrification and disposed of in repositories. Recently, another option, the recovery of Np from HLLW, has become of increasingly interest, as (1) the long term radiotoxicity of nuclear wastes in the repositories could be dramatically decreased; and (2) ^{237}Np can be used to produce ^{238}Pu, a heat source for radioisotope thermoelectric generators [1].

The different valences of Np (+3 to +7) present their different chemical behaviors. In solutions, trivalent Np is a strong precarious reducing agent and readily oxidized to the tetravalent state. As a result, trivalent Np only exists in de-aerated environments. Heptavalent Np may exist as NpO_2^{3+} in acidic solutions but NpO_2^{3+} could be reduced to NpO_2^{2+} within minutes. Only under basic conditions (0.1 - 2 M KOH) may heptavalent Np be stabilized under the chemical form of NpO_6^{5-} [1,2]. Throughout the PUREX process, Np^{4+}, NpO_2^+, and NpO_2^{2+} are the existing Np species in acid-dissolved solutions of UNF. Their effective extraction largely follows the order: $Np^{4+} > NpO_2^{2+} \sim Np^{3+} > NpO_2^+$. Although Np is, in principle, intended to be treated as HLLW in the context of the PUREX process, it is impossible to expel all Np (in reality ~1/3 of Np [3,4]) into the HLLW stream after the first cycle, the U-Pu co-extraction cycle, because of the inter-transformations among the different valences (**Figure 1**). At operating acidities of the PUREX process (1~5 M HNO_3), most Np exists as NpO_2^+ and NpO_2^{2+}, due to the oxidation by HNO_3 and its endogenous radiolysis products such as HNO_2 and $\cdot NO_3$. Over the 2.5~3 M HNO_3 range, ~90% Np exists as NpO_2^{2+} and Pu remains in the +4 oxidation state, as NO_3^- stabilizes Pu^{4+} and prevents its oxidation to PuO_2^{2+} [2]. The Np^{4+} content is relatively low but can become important enough upon the addition of reductants (e.g. U^{4+}) to enable separation from its neighboring actinides. Np^{4+} follows UO_2^{2+} into a second cycle that is then necessary to purify U. NpO_2^{2+}, if not reduced, is also co-extracted by TBP in paraffinic hydrocarbon (e.g. *n*-dodecane or kerosene) along with residual unreduced Pu^{4+} and UO_2^{2+} from the first cycle. The higher the acidity is, the greater the $[HNO_3]/[HNO_2]$ ratio is, and consequently the larger the $[NpO_2^{2+}]/[NpO_2^+]$ ratio is.

This pattern is due to the dual functions of HNO_2, which reduces NpO_2^{2+} to NpO_2^{+} at high concentrations (Equation 1) and catalyzes the oxidation of NpO_2^{+} to NpO_2^{2+} at low concentrations as shown below [5]. In the second cycle where U and Np are separated from Pu, reduction of Pu^{4+} to Pu^{3+} followed by stripping into the aqueous phase is achieved either by introducing reducing agents such as ferrous sulfamate, hydroxylamine, and U^{4+}, or by inducing cathodic reduction. Both the mass-separating and the energy-separating agents suffer from slow kinetics to reduce NpO_2^{+} (an intermediate from the reduction of NpO_2^{2+}) to Np^{4+} within a time frame comparative to that of Pu^{4+} reduction [2], resulting in a mixture of all three oxidation states. Another component that complicates Np behavior is HNO_3. HNO_3 plays a dual role in the redox chemistry of Np by oxidizing Np^{4+} to NpO_2^{+}, and then to NpO_2^{2+} (Equation 2), and by stimulating the disproportionation of the produced NpO_2^{+} at high acidities (Equation 3). Depending on the amount of HNO_3, HNO_2, and their radiolysis products, a mixture of Np species with different valences ensues, making recovery especially difficult.

$$2NpO_2^{2+} + HNO_2 + H_2O \leftrightarrow 2NpO_2^{+} + 3H^{+} + NO_3^{-} \quad \textbf{(Eq. 1)}$$

$$2Np^{4+} + NO_3^{-} + H_2O \leftrightarrow 2NpO_2^{+} + HNO_2 + 5H^{+} \quad \textbf{(Eq. 2)}$$

$$2NpO_2^{+} + 4H^{+} \leftrightarrow Np^{4+} + NpO_2^{2+} + 2H_2O \quad \textbf{(Eq. 3)}$$

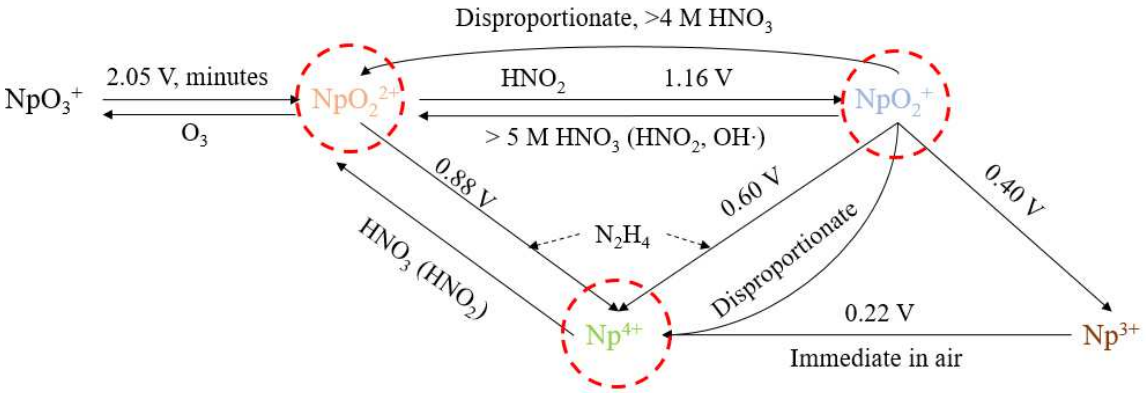

Figure 1. Transformations among different valences of Np. The standard reduction potentials are versus SHE [1], colored species are those found in acidic media, and circled ions are those PUREX-relevant species.

The Adapted PUREX process was brought forward with the aim to route Np more precisely. Four routes of Np have been proposed for Np [1], of which two are routing all Np to the HLLW stream preceding the second cycle and to the stripping raffinate of the second cycle before U-Pu separation. These two options are not desirable since accurate reduction to NpO_2^{+} is hard to

control and may affect Pu valence, unless Pu is directed into the HLLW, such as in the URanium Extraction (UREX) process [6]. Following U would cause proliferation issues since pure Pu can be produced. Hence following Pu is most favorable and has been adopted in the United Kingdom under the Advanced PUREX process [5] and in France under the COEX process [7]. In the U purification cycle where Pu and Np (if Np is chosen to follow Pu in lieu of U) are separated from U, reductants (e.g. $Fe(NH_2SO_3)_2$, U^{4+}, N_2H_4, or NH_2OH) are added to reduce Pu^{4+} to Pu^{3+} and NpO_2^{2+} to NpO_2^{+}. Np^{4+} may be formed, although the reduction kinetics are slow, which makes Np coexist with U and degrades the U purification efficiency. The Np-Pu mixture does not necessarily entail separation in view of proliferation. Successive addition of oxidizers (e.g. H_2O_2) and reductants (e.g. N_2H_4) permits the adjustment of most of Np and Pu to Np^{4+} and Pu^{4+}, which are then purified as a whole from impurities (e.g. Fe and Tc) [8]. If Pu needs to be separated from Np in the second cycle, Np-Pu mixture discharged from U/Pu separations are re-oxidized to NpO_2^{+} and Pu^{4+}, with NpO_2^{+} and impurities staying in the aqueous phase while Pu^{4+} is extracted into the organic phase. Then one more redox step is performed to separate Np from impurities. When separation of Pu from Np is desired, the formation of Np^{4+} can accompany Pu^{4+}, and thus downgrading the quality of the Pu product. The Np valence in the HLLW stream can be controlled in a similar way as demonstrated in the TRUEX process, where NpO_2^{+} is transformed to either NpO_2^{2+} or Np^{4+}, then extracted by octyl(phenyl)-N,N-diisobutylcarbamoylmethylphosphine oxide (CMPO) [4].

Many attempts have been made to control the valences and thus the routes of Np, of which most were focused on selecting appropriate reductants. So far the salt-free candidates are (iso-)butyraldehyde, hydrazine and hydroxylamine and their derivatives, hydroxamic acid, and (di-)hydroxyurea [9]. All of the above have only reducing capability, except hydroxamic acids (such as acetohydroxamic acid (AHA) and formohydroxamic acid (FHA)) that bear both redox and complexation capabilities [9,10]. Another trait that makes hydroxamic acids stand out is the ensuing negligible extractability by TBP [9]. In the UREX process and its variants adopted in the U.S. or in the Advanced PUREX adopted in the U.K. [11], U is extracted by TBP while Np and Pu are both scrubbed into the aqueous phase using AHA as the aqueous complexant that retains the tetravalent forms of the metals. AHA can also reduce NpO_2^{2+} to NpO_2^{+} and expel the latter from the organic phase [12], which offers some advantage over other Np chelators (e.g. $(COOH)_2$, CO_3^{2-},

ethylenediaminetetraacetic acid (HEDTA) [1], or diethylenetriaminepentaacetic acid (HDTPA) [13]) that do not possess redox capabilities, and over certain NpO_2^{2+} reductants that do not form complexes. However, AHA cannot reduce NpO_2^{2+} or NpO_2^{+} to Np^{4+} and complex Np^{4+} at the same time. As a result, in a mixture of Np species with different valences, the controlled efficiency of AHA is restrained. Citrate, a chelator commonly used as buffer, can also reduce both dioxo species to Np^{4+} and complex them, although with a very slow reaction rate (197 days to reduce ~1/3 NpO_2^{2+} to Np^{4+}) [14]. However, its efficacy at high acidities remains questionable since such a study was performed at pH 6 [14]. Finally, the DIDPA process developed by the Japanese Atomic Energy Agency leverages the extraction of NpO_2^{+} into the organic phase using diisodecylphosphoric acid (DIDPA), but results in incomplete recoveries [1]. A chelator that can reduce neptunyl to and complex Np^{4+} at high acidities with fast kinetics is therefore desired for Np separation.

Previous studies have shown that the hydroxyl group in the reductant molecule enhances the kinetics and that the complex stability increases linearly as the number of metal-bound donor atoms increase [1]. A CHON-based octadentate chelator called 3,4,3-LI(1,2-HOPO) (referred to as HOPO, **Figure 3**) is comprised of four acidic carboxylic groups and four tertiary amine groups, and is known for its extremely high affinity towards M^{4+} ions [15,16]. Hence HOPO is likely to effectively adjust and stabilize the valence of Np, and is completely burnable, which helps minimizing the generation of secondary waste. In this work, extraction profiles of U, Np, and Pu were determined by radiometric methods as a function of pH. Valence profiles of Np and Np-HOPO complexes were analyzed by absorption spectrophotometry using UV-vis-NIR. Although some other techniques have much higher sensitivities to monitor Np species, such as laser induced photoacoustic spectroscopy adopted in the PUREX process [17], traditional direct absorption spectrophotometry is simple, rapid, and easy to implement on benchtop, and thus adopted here. The redox properties were probed by cyclic voltammetry (CV). The redox couples of NpO_2^{2+}/NpO_2^{+} and of Np^{4+}/Np^{3+} were characterized as Nernstian in $HClO_4$ and HNO_3 and as irreversible in H_2SO_4 and CH_3COOH [1,18]. Recently, NpO_2^{2+}/NpO_2^{+} was found to change from Nernstian to quasi-reversible (QR) in HNO_3 media when the nitrate concentration decreased [19]. The kinetics of these two redox couples were also investigated and the reaction proceeded by an outer-sphere mechanism [20]. In contrast, NpO_2^{+} reduction to Np^{4+} is theoretically irreversible due

to the structural change from linear transdioxoneptunyl ions to spherical aquo-coordinated ions in aqueous media [19] and the redox properties of the NpO_2^+/Np^{4+} couple are hard to analyze by conventional electrochemical techniques since rupture or formation of the Np-O bonds of is slow [1,21]. Gibbs energies of formation are therefore the recourse to obtain the standard reduction potentials [1]. The only reported CV result for the NpO_2^+/Np^{4+} couple was inferred from its counterpart couples instead of direct observation [22]. The scarcity in studies of the NpO_2^+/Np^{4+} couple motivated the redox studies reported herein and the subsequent evaluation of the Np-HOPO interaction.

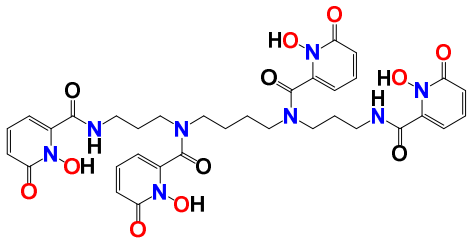

Figure 2. Molecular structure of 3,4,3-LI(1,2-HOPO).

Materials and Methods

Caution! *All isotopes used in this study, $^{233}UO_2^{2+}$ ($t_{1/2}=1.59\times10^5$ y, 9.7×10^{-3} Ci/g), $^{237}NpO_2^+$ ($t_{1/2}=2.14\times10^5$ y, 7.1×10^{-4} Ci/g), $^{232}Th^{4+}$ ($t_{1/2}=1.40\times10^{10}$ y, 1.1×10^{-7} Ci/g) and $^{242}Pu^{4+}$ ($t_{1/2}=3.74\times10^5$ y, 3.9×10^{-3} Ci/g) are hazardous and radioactive materials with high specific radioactivities and should be handled only in specifically designated facilities in accordance with appropriate safety controls.*

Chemicals. HOPO was obtained from Ash Stevens, Inc. (Detroit, MI) and its aqueous stock solutions with varied concentrations were prepared by direct dissolution in water prior to each sets of experiments. HNO_3 (70%, 6 M, and 0.1 M) was purchased from Sigma-Aldrich, VWR BDH, and MilliporeSigma (Billerica, MA), respectively; $NaNO_3$ with >99% purity from Alfa Aesar (Ward Hill, MA); kerosene from Alfa Aesar (Heysham, U.K.); and Ultima Gold™ from Perkin Elmer Inc (Waltham, MA). TBP was from Sigma-Aldrich and used as received. The $^{237}NpO_2^+$ stock in 0.01 M HCl was sourced from an in-house stock of the Heavy Element Research Laboratory (HERL) at the Lawrence Berkeley National Laboratory (LBNL). The Np concentration in the stock was determined prior to use to be 29.71 mM by measuring the maximal absorbance at the maximal wavelength, λ_{max}, of 980 nm (maximal molar attenuation

coefficient, ε_{max}=395 abs/(M·cm)) using a Varian Cary 6000i UV−Vis−NIR double-beam spectrophotometer. A ^{232}ThCl stock in 0.1 M H_2SO_4 was adopted directly from in-lab inventory [23]. The Pu concentration of the in-house $^{242}Pu^{4+}$ stock in 0.5 M HCl was determined to be 25.32 mM in the same way as that employed for the $^{237}NpO_2^+$ stock. The purity of all isotopes was evaluated by gamma spectroscopy using a high purity solid-state Ge γ-spectrometer (Ametek Ortec, TN). A Millipore Milli-Q Advantage A10 Water System Production unit was used to purify deionized water before preparing all aqueous solutions.

Liquid-liquid extraction. Extraction experiments were performed with a series of acidities in the aqueous phase at ambient temperature in triplicate. The acidities were controlled by varied HNO_3 concentrations. Each extraction consisted of the following three steps: (i) Conditioning: Organic phases were contacted with the aqueous phases holding appropriate acidities for 10 min (phase volume ratio, defined as the organic-to-aqueous volume ratio, V_o/V_a=1). (ii) Extraction: a 2-μL radiotracer solution was pipetted into a vial holding 398 μL of the aqueous phase, a 400-μL conditioned organic phase was then added, and the vial was shaken for 10 min. (iii) Counting: 200-μL aliquots were taken from each phase after phase separation by centrifugation (5 min at 3000 rpm) and then added to a scintillation vial with 10 mL scintillation cocktail (Ultima Gold, Perkin Elmer, CT, USA). Scintillation counting was conducted on Packard Tri-Carb model B4430 (Perkin Elmer).

Three parameters were used to characterize the extraction performance: the distribution ratio (D, Equation 4) in terms of count rate (R_c) with the unit of count per minute (cpm), the extraction fraction (E, Equation 5) calculated from D and the phase volume ratio V_o/V_a, and the separation factor (SF, Equation 6).

$$D_M = \frac{[M]_{tot,org}}{[M]_{tot,aq}} \propto \frac{R_{co}}{R_{ca}} \quad \textbf{(Eq. 4)}$$

$$E = \frac{D_M}{D_M + V_a/V_o} = \frac{1}{1 + 1/D_M} \quad \textbf{(Eq. 5)}$$

$$SF_{M_1/M_2} = D_{M_1} / D_{M_2} \quad \textbf{(Eq. 6)}$$

UV-Vis-NIR spectrophotometry. All spectra were collected on a Varian Cary 6000i UV−Vis−NIR double-beam spectrophotometer using a 1 cm quartz cuvette. A solution of 1 M HNO_3 was prepared as the background solution and its spectrum was taken as the reference. Three solutions with three different analytes were prepared in 1 M HNO_3, one with 1 mM HOPO, one with 0.75 mM NpO_2^+, and the third one with 0.75 mM Np-HOPO complex. When the first two solutions were prepared, an aliquot of 0.05 mL of NpO_2^+ stock solution was added into a 1.95 mL background solution separately such that the 2-mL sample contained 0.75 mM NpO_2^+. The HOPO solution followed exactly the same procedure. When the third solution was prepared, aliquots of 0.05 mL for NpO_2^+ and HOPO were added into a 1.90 mL background solution such that the final solution contained an equal molar of 0.75 mM of both NpO_2^+ and HOPO. The band range was from 1100 to 280 nm stepwise with a data interval of 1 nm. The existence of NO_3^- did not mask the UV region since its absorption was at λ_{max} = 240 nm. All steps were performed at ambient temperature.

Cyclic voltammetry (CV). A compact voltammetry cell with a screen-printed glassy carbon electrodes (SPCarEs) card was connected to a Wavenow potentiostat. The SPCarEs card included a carbon working electrode (rectangular, 4×5 mm), and a carbon counter electrode. The reference electrode was Ag/AgCl/$KCl_{sat'd}$ (E = 0.199 V vs NHE) and all potentials values hereafter refer to Ag/AgCl. All above-mentioned parts were manufactured by PINE Research. The SPCarEs card does not have the problem of H^+ adsorption as for the Pt electrode. However, its working electrode is prone to slow heterogeneous kinetics due to carbon ink binders that shelter electroactive carbon particles, so activation of the carbon surface is needed. Cycling in 0.1 M H_2SO_4 to extreme potentials (-2.5 to 2.5 V) was used herein due to its simplicity. Three aqueous electrolyte solutions were prepared, with the analyte respectively being 1 mM HOPO, 0.25 mM NpO_2^+, and 0.25 mM Np-HOPO complex, all in the same supporting electrolyte of 1M $NaNO_3$ and 1 M HNO_3 and the same solvent of H_2O. The electrolyte solutions were scanned at varied scan rates from 0.01 V/s to 0.4 V/s at 25°C. The calculations of kinetic and thermodynamic parameters are detailed in the ESI.

Metal competition titration. The methodology is by and large the same as for previously reported systems [23–27]. Two M^{4+} ions (M = Th, Pu), both being 0.5 mM in 1 M HNO_3, were used

individually to compete with Np^{4+} in complexing HOPO. A 1 mL solution initially containing 25 μM NpO_2^+ and equimolar (1 eq) HOPO in 1 M HNO_3 was prepared and left vernight to allow the reduction of NpO_2^+ and the complexation of Np^{4+} to reach equilibrium, although the reactions are fast as indicated in other experimental results [21]. The NpHOPO complex solution was then transferred into a screw-cap quartz cuvette with a path length of 1 cm for absorbance measurements. Incremental addition of M^{4+} in 1 M HNO_3 were performed from 0 to 4 equivalents and the corresponding absorbance spectra were recorded 10 min after each addition although we observed the equilibrium was reached nearly within 1 min in a preliminary study. The spectra of M^{4+}, MHOPO, and NpHOPO were also recorded for data fitting. All spectra were collected at room temperature, from 300 to 500 nm, using a Varian Cary 6000i UV−Vis−NIR double-beam spectrophotometer, and were corrected by a blank of 1 M HNO_3.

Data treatment. Spectrophotometric titration spectra were imported into HypSpec [28] and deconvolution was accomplished by nonlinear least-squares analysis, to refine the cumulative formation constant of the NpHOPO complex. The cumulative formation constant, β_{mhl}, is defined in Equation 7, where M, H, and L designate metal, proton, and ligand, respectively.

$$mM + hH + lL \xleftrightarrow{\beta_{mhl}} M_m H_h L_l \text{ , } \beta_{mhl} = \frac{[M_m H_h L_l]}{[M]^m [H]^h [L]^l} \quad \textbf{(Eq. 7)}$$

All metal and ligand stock concentrations were held constant at values determined from the volume of standardized stock solutions. All species formed with HOPO had significant absorbance in the wavelength region of interest and were included in the refining process. Therefore, the following chemical equilibria were considered: HOPO protonation, metal complexation with HOPO, and metal complexation with nitrate due to the high concentration of HNO_3. The autoprotolysis of H_2O and the hydrolysis of M were ignored due to the high acidity (1 M HNO_3) in which the titration was accomplished. The values of the formation constants of the HOPO protonation and the MHOPO complexation were taken from the results of our previous studies [23,29,30] and fixed in the fitting process; those of nitrate complexes were taken from the literature [31] (**Table S3**). Speciation was calculated using HYSS [28] and no hydroxide species existed under the experimental acidity. Uncertainties on $\log\beta_{mhl}$ and pK_a values presented

in this paper correspond to the standard deviation observed over two replicates of the spectrophotometric measurement and the data treatment.

Results and Discussion

Liquid-liquid extraction experiments. Before adding HOPO in the aqueous phase, the extraction percentage by TBP increased with the nitric acid concentration, as shown by the solid lines in **Figure 3**, most evidently for Np and least for U. This is because increasing acidity boosted the concentration of NO_3^- and TBP is a neutral solvating extractant, so the same ion effect enhanced the extraction via the reactions depicted by Equations 8 and 9.

$$\begin{cases} MO_2^{2+} + 2HNO_3 + 2TBP \longleftrightarrow MO_2\left(NO_3\right)_2 \cdot 2TBP + 2H^+, M = U, Np \\ M^{4+} + 4HNO_3 + 2TBP \longleftrightarrow M\left(NO_3\right)_4 \cdot 2TBP + 4H^+, M = Np, Pu \end{cases} \quad \textbf{(Eq. 8 \& 9)}$$

At constant acidity, TBP showed different affinities to different metal ions in the order of UO_2^{2+}~Pu^{4+}>>NpO_2^+ ions. The high affinities for UO_2^{2+} and Pu^{4+} ions resulted in the extraction percentage being nearly 100% when the HNO_3 concentration was > 2 M. As opposed to these two elements with mildly growth in the extraction, Np displayed a sudden escalation when the HNO_3 concentration is > 4 M in a non-complexing medium. One reason is the NO_3^- effect mentioned above. Another reason is that high concentrations of HNO_3 and HNO_2 promoted the disproportionation of NpO_2^+ to NpO_2^{2+} and Np^{4+}, which are much more extractable than NpO_2^+. Therefore, the starting solution of pure NpO_2^+ became an apportioned mixture of Np^{4+}, NpO_2^+, and NpO_2^{2+}, resulting in higher extraction. To single out Np, the PUREX process adjusts the acidities and needs reductants to control the valences of Np. This introduces extraneous chemicals as well as more steps. Our goal is to use HOPO to suppress the co-extraction of Np with UO_2^{2+} and Pu^{4+} ions at high acidities that conform to PUREX conditions.

Upon adding HOPO, the UO_2^{2+} extraction remained undisturbed, consistent with previously reported results from our group [16]. In contrast, the extractions of Pu and Np were prominently suppressed to an extent that virtually no extraction was observed (dashed lines, **Figure 3A**). With the weaker complexing capability of HOPO for the pentavalent actinyl species, we suspect NpO_2^{2+} was reduced to Np^{4+} and the high stability constant of Np^{4+}-HOPO complexes prevailed

over Np^{4+}-TBP interactions, resulting in the practically complete binding of Np in the aqueous phase, as shown in **Figure 3A**. Valence states determination entails other techniques, UV-vis-NIR spectroscopy and CV, which are elaborated upon herein. The distribution ratio of each element is shown in **Figure S1** and the separation between pairs among the three elements is shown in **Figure 3B**. As the acidity increased, HOPO drastically enhanced U/Np (up to ~90 fold by 8 M HNO_3) and U/Pu (up to ~10300 fold by 8 M HNO_3) separations, while it reduced that of Pu/Np (decreased to ~0.01 by 8 M HNO_3), all compared to the values obtained using conventional PUREX formulae.

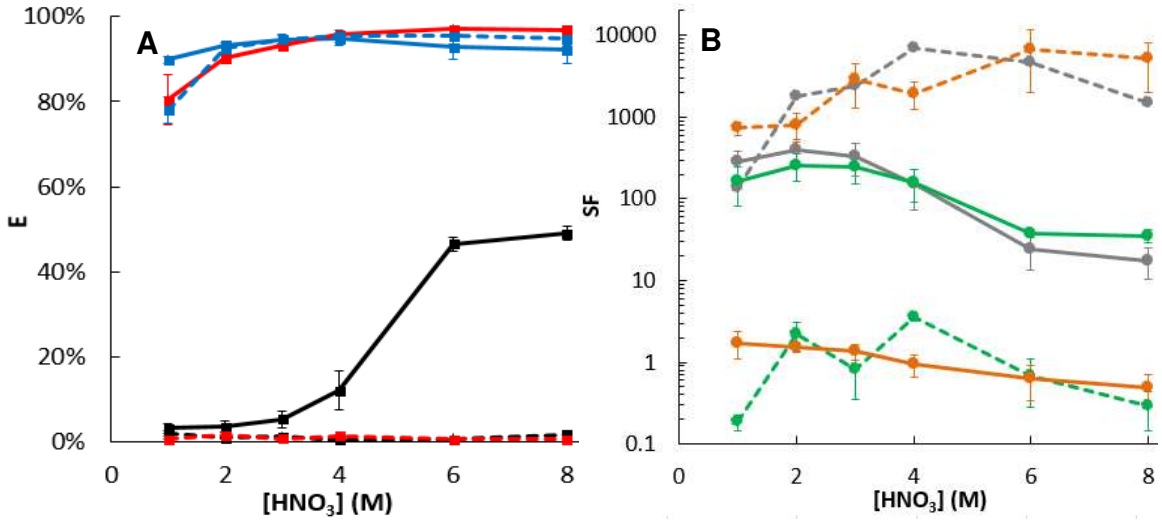

Figure 3. (A) Extraction of UO_2^{2+} (blue), NpO_2^+ (black), and Pu^{4+} (red) by TBP as a function of nitric acid concentrations with (dashed lines) and without (solid lines) HOPO in the aqueous phase. Organic phase: 30 v% TBP in kerosene. Aqueous phase: 0 or 1 mM HOPO in varied concentrations of HNO_3 and 1 M $NaNO_3$. V_o/V_a = 1. U (blue), Np (black), Pu (red). **(B)** Corresponding SF values of UO_2^{2+} and Pu^{4+} from NpO_2^+. SF(U/Np) (gray), SF(Pu/Np) (green), SF(U/Pu) (orange).

The influences of HOPO on the separation performance can be clearly seen from the transition from solid curves (no HOPO) to dashed curves (1 mM HOPO) in **Figure 3**. Among the three elements of concern (U, Np, and Pu) that form three pairs to investigate, the separations of Np from U (U-Np pair) and of Pu from U (U-Pu pair) were both greatly improved upon the addition of HOPO. In stark contrast, the separation of Np from Pu (Np-Pu pair) was exacerbated. In the U purification cycle of the PUREX process, HOPO can be a potentially effective recourse to achieve a better separation of Np and Pu from U by promoting the separation factors, while paring the demands for reducing agents and dilute HNO_3 to adjust the valences of Pu and Np. Thus, fewer stages are needed to purify U and downstream regeneration is much easier. In order to separate Np from Pu in the second cycle of Pu purification, the solution pH can be adjusted to

near neutral range to precipitate the Np^{4+}-HOPO complex [32]. **Figure 4** displays the proposed modification to the existing Adapted PUREX process. Note that the separation of Np from Pu is unnecessary if MOX fuel is to be fabricated for fast reactors [9]. Of note, real dissolved use fuel solutions have high metal loadings and impurities (e.g. fission products) that may alter the performance of HOPO. Further studies are thus warranted, with continuous extraction and different metal loading ratios and concentration, to determine the robustness of the proposed process.

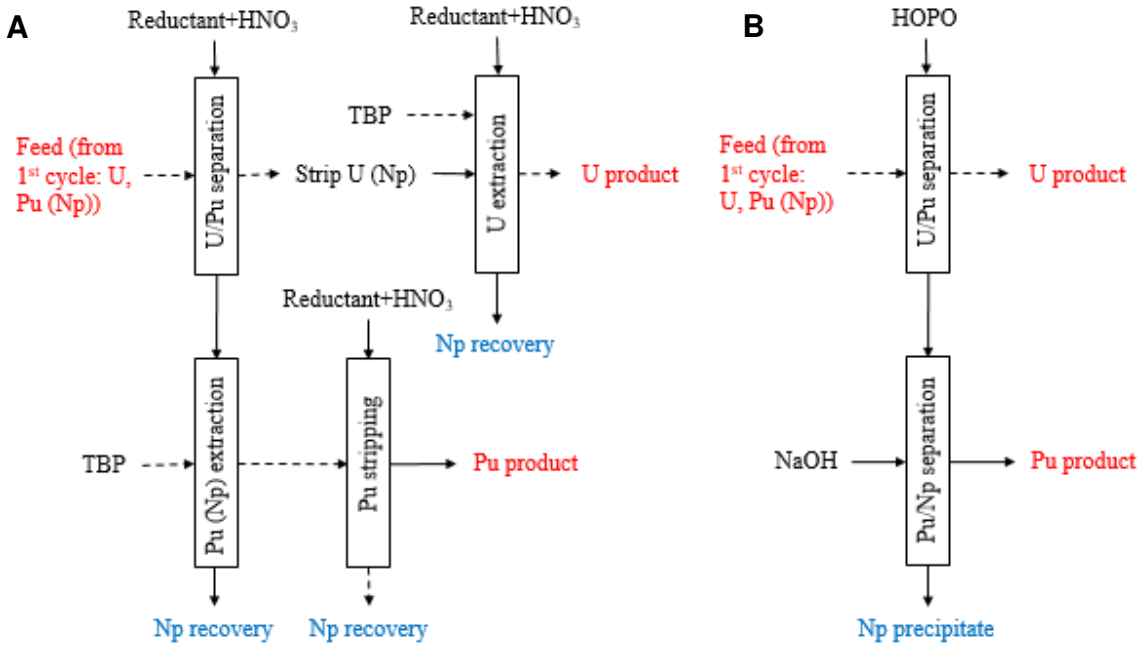

Figure 4. Schematic flow sheets of the PUREX process (A) and proposed Adapted PUREX process (B). → aqueous stream, ···> organic stream.

UV-Vis-NIR spectrophotometry. The redox interactions between NpO_2^{2+} and HOPO were studied by absorption spectrophotometry. **Figure 5** shows a sharp band, representative of NpO_2^+, centered at λ_{max} = 980 nm, as a result of the vibration of the dioxo bonds of neptunyl ions. Another sharp band at λ = 617 nm is much weaker, stemming from an *f-f* transition that is Laporte forbidden. NpO_2^+ almost has no absorption of light at other wavelengths in the vis-NIR region. The observed spectrum agreed well with the reported results wherein it was also reported that the HNO_3 concentration was not a significant factor in the range of 1~6 M [33]. Free HOPO had a strong absorption in the near UV region and exhibits a sharp peak at λ_{max} = 350 nm due to

the $\pi \rightarrow \pi^*$ transition of the ligand unsaturated bonds, while it does not show any sign of light absorption in either visible or NIR region.

When NpO_2^+ and HOPO were mixed together, the characteristic peaks centered at 980 nm of NpO_2^+ disappeared almost instantaneously, suggesting the occurrence of Np(V) reduction. This is contrary to the expected slow reduction kinetics known for breaking the Np-oxo bond. In the near UV region of 300 - 400 nm, where the charge transfer band located, the charge re-distributed between Np and HOPO and resulted in conspicuous features. The absorption of the complex became tremendously stronger (ε_{max} = 7470 abs/(M·cm)) than the HOPO peak centered at λ_{max} = 335 nm; meanwhile the curvature of HOPO also changed. In the vis-NIR region, the formed complex displayed two broad peaks centered at λ = 740 and 990 nm with about the same absorbance but the magnitude is considerably smaller (ε_{max} = 48 abs/(M·cm)) than that of NpO_2^+ (ε_{max} = 395 abs/(M·cm), reported value [1]), only about 1/10 of the latter. A small ε_{max} value is usually the sign of the *f-f* transition of metal ions in the coordination field since this type of transition is Laporte forbidden. Such a phenomenon is commonly encountered in many An^{4+} species. While the observed peak at λ = 990 nm might be the red-shift result upon the formation of pentavalent Np-HOPO complex, the peak centered at λ = 740 nm cannot be explained properly. Therefore, the valence of Np is likely to change upon interactions with HOPO. Np^{4+} has two characteristic peaks centered at λ = 710 (ε=125 abs/(M·cm)) and λ_{max} = 960 nm (ε_{max}=165 abs/(M·cm)), and the two broad peaks developed at λ_{max} = 740 nm and λ = 990 nm can be reasonably deduced to be the red-shift results of Np^{4+} upon its complexation with HOPO. Namely NpO_2^+ was reduced by HOPO to Np^{4+} that was complexed by HOPO as soon as it was formed. Our group has observed the reduction of NpO_2^{2+} and NpO_2^+ before by Raman spectroscopy [32] and X-ray absorption spectroscopy [21], and the results herein confirms such reduction reaction.

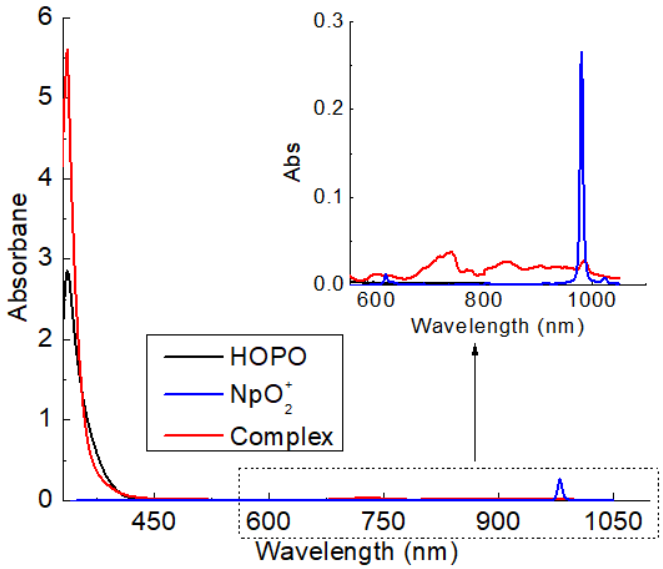

Figure 5. Spectrum of NpO_2^+, HOPO, and Np-HOPO complex; 0.75 mM in background solutions that contain I = 1 M HNO_3.

Cyclic voltammetry. The following electrochemical reactions are brought forward as the mechanism for the reduction of NpO_2^+ by HOPO:

$$Anode: HOPO_R - e^- \leftrightarrow HOPO_O$$
$$Cathode: NpO_2^+ + 4H^+ + e^- \leftrightarrow Np^{4+} + 2H_2O \qquad \textbf{(Eq. 10, 11, \& 12)}$$
$$Overall: NpO_2^+ + HOPO_R + 4H^+ \leftrightarrow Np^{4+} + HOPO_O + 2H_2O$$

A previous study showed that an O atom on one of the 1,2-HOPO moieties was oxidized at pH = 4.5 in H_2SO_4 medium and an anodic peak was produced, and also showed that no reduction was observed [21]. To analyze these interactions under reprocessing-relevant conditions, all electrolyte solutions were prepared in 1 M HNO_3. A preliminary CV result at a scan rate (v) of 0.05 V/s (**Figure S2**), demonstrated that HOPO can be both oxidized and reduced, so we deduce that the O atom in the 1,2-HOPO moiety can be not only oxidized but also reduced when the acidity condition is changed. The peak-to-peak separation potential (ΔE_p, defined as E_{pa}-E_{pc}) of HOPO was 0.125 V, much larger than the theoretical value of 0.057 V for a Nernstian process with single electron transfer [34,35]. Therefore, HOPO exhibits a quasi-reversible (QR) behavior under these new experimental conditions. The half-wave potential ($E_{1/2}$, defined as $(E_{pa}+E_{pc})/2$), approximately equal to the formal potential ($E^{o'}$) by assuming the same diffusion coefficient of a redox pair, was about 0.36 V. In contrast, the NpO_2^+/Np^{4+} couple exhibited a Nernstian trait (consistent with spectrophotometric results) with a ΔE_p = 0.05 V (close to 0.057 V) and $E_{1/2}$ =

0.40 V. No other valences of Np were observed. The Np-HOPO complex displayed a shift of the anodic peak toward positive values and of the cathodic peak towards negative values. A ΔE_p value of 0.14 V was also much larger than 0.057 V, indicating a QR process, with a corresponding $E_{1/2}$ = 0.40 V. Neither multiple complex species nor multistep electron transfer processes was observed within the scanned potential range.

To better assess the chelation-driven reduction, the thermodynamics and the kinetics of such metal-ligand interactions were tentatively evaluated by collecting the scans of HOPO, NpO_2^+, and Np-HOPO complex under various v (including 0.05 V/s in **Figure S2**). **Figure 6** shows the i~E traces of HOPO, NpO_2^+, and Np-HOPO complex, from which ΔE_p and the half-wave potential, $E_{1/2}$, can be calculated. As a result, certain kinetic and thermodynamic parameters were evaluated by Nicholson's method [36] and Nernst equation, respectively.

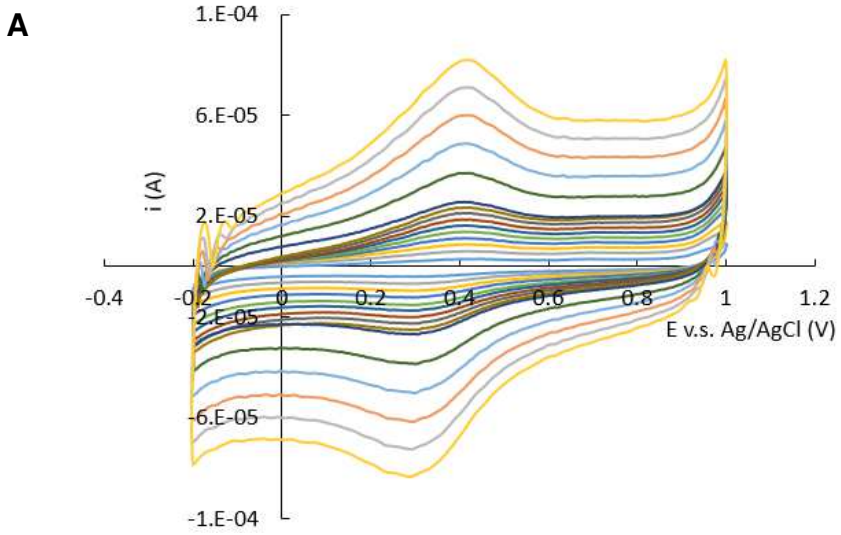

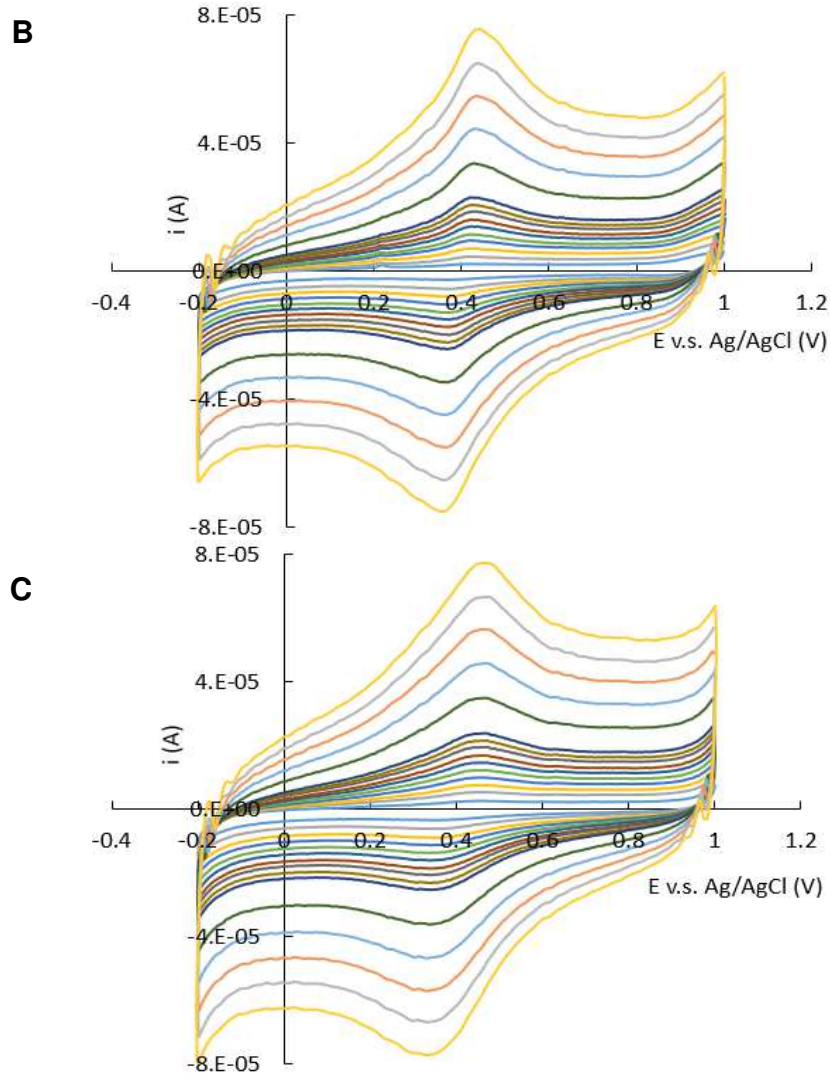

Figure 6. CV of 1 mM HOPO (A), 0.25 mM NpO_2^+ (B), and 0.25 mM Np-HOPO (1:1) complex (C) in 1 M HNO_3 solution under varied scan rate from 0.01 V/s to 0.4 V/s.

The computed ΔE_p values are plotted against v as illustrated in **Figure 7**. The ΔE_p values of HOPO were centered around 0.12 V and did not shift with v, which means that there existed specific surface-adsorbed species [35]. When v is small both dissolved and adsorbed species were electroactive. Since neither prepeak nor postpeak was observed during the whole cycle no strong absorption existed, and since both the cathodic and anodic peak increased to roughly the same degree both the reactant and the product were weakly adsorbed. At faster scan rates, only adsorbed species are electroactive and ΔE_p should be 0 for a Nernstian process, which is obviously the case here. The process is likely to be QR instead of irreversible at high v since both cathodic and anodic peaks were observed. On the contrary, most ΔE_p values of NpO_2^+ were

close to 0.057 V at v < 0.1 V/s, which indicated that the charge transfer was facile and that NpO_2^+ was reduced to Np^{4+} via an electrochemically reversible step under these experimental conditions. As v went above 0.1 V/s, the current augmented due to the curtailed thickness of the diffusion layer. Meanwhile the barrier of electron transfer became higher and the process became slow, signifying a transition to a QR process where more negative/positive potentials (thus greater ΔE_p) were needed to drive the reduction/oxidation. The ΔE_p values of the Np-HOPO complex kept relatively constant and approximately the same as those of HOPO. Similar to HOPO, the Np-HOPO complex system showed weak specific adsorption. The standard heterogeneous rate constant, k_0, of the electrochemical reaction of each redox pair can be evaluated from ΔE_p based on Nicholson's method for QR processes and plotted against $v^{1/2}$ (**Figure 8**), to reflect the distinction degree of ΔE_p. The more uniformly ΔE_p is dispersed, the higher the linearity is. The calculated values of both Λ and k_0 falls into the ranges corresponding to a QR process, confirming both HOPO and Np-HOPO exhibit a QR behavior. The detailed calculation steps are provided in the supporting information. The k_0 value determined for the Np redox couple was roughly 10 to 20 times greater and fairly uniform since the system was Nernstian and in transition to QR. The calculated results are not shown here since they were estimated by the method that is, strictly speaking, applicable to QR systems only.

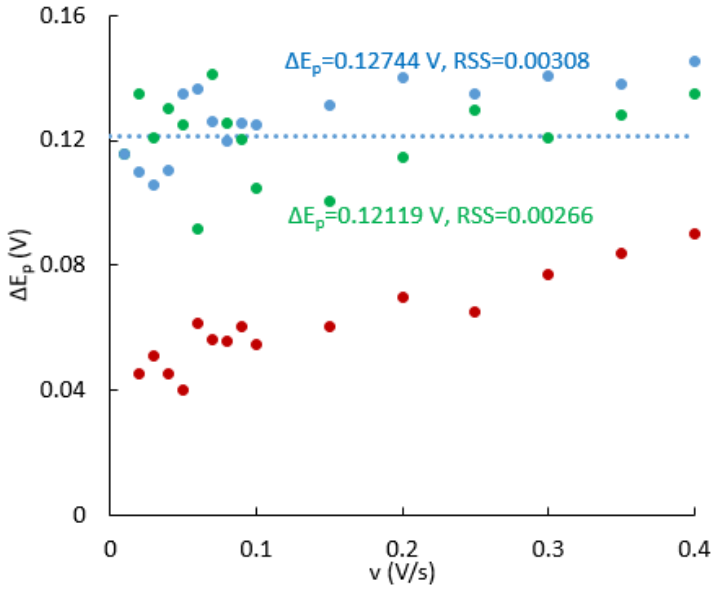

Figure 7. Dependence of the peak-to-peak separation potential, ΔE_p, of NpO_2^+ (magenta), HOPO (green), and Np-HOPO complex (blue) as a function of the scan rate, from 0.01 V/s to 0.4 V/s, in 1 M HNO_3 solution.

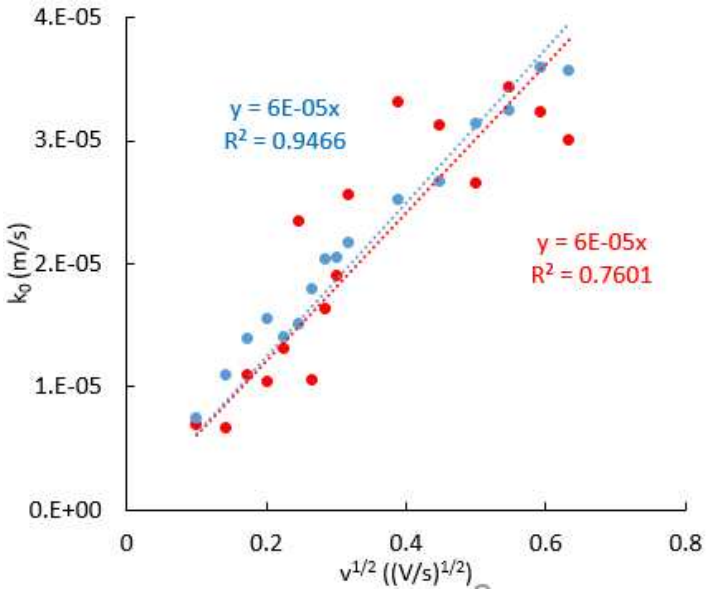

Figure 8. Dependence of the calculated heterogeneous rate constant, k_0, of the electrochemical reactions of HOPO (red), and Np-HOPO complex (blue), as a function of the scan rate, from 0.01 V/s to 0.4 V/s, in 1 M HNO_3 solution. The corresponding linear fittings are for the free HOPO ligand (red dash line) and the Np-HOPO complex (blue dash line). Np is excluded since its reaction is not a QR process.

The $E_{1/2}$ values can be adopted to shed some light on the thermodynamics of Np-HOPO interaction since $E_{1/2}$ can be used to calculate the electromotive force, E_{MF}, and the free energy, ΔG, of the interaction reaction. **Figure 9** shows that $E_{1/2}$ is oscillating around 0.40 V for Np and the Np-HOPO complex, while it is around 0.35 V for the free ligand. This results in a positive formal E_{MF} ($E^{o'}_{MF}$) of c.a. 0.05 V and thus a negative ΔG value, which is consistent with the overall reaction described by Equation 12. Of note, this is by no means a guaranteed indicator of the occurrence since whether or not the reaction happens is dictated by E_{MF} that is influenced by not only $E^{o'}_{MF}$ but also the chemical environment. The exact E_{MF} can be calculated by the Nernst equation and it turned out that the higher the acidity is the more likely the overall reaction is to proceed. This helps explain the observed extraction behavior. In addition to the dual roles of HNO_3 discussed in the extraction section, high HNO_3 concentration can also increase E_{MF}, rendering more positive values and thus facilitating the reduction process. Since reduced Np^{4+} formed the Np^{4+}-HOPO complex, which overwhelmed Np-TBP complexation, the extraction of Np was curbed. E_{MF} can be further increased upon the complexation if the reduced form is more stable than the oxidized form. However, although the Np^{4+}-HOPO complex is much more stable than NpO_2^+-HOPO, the effect was negligible because the concentration difference between the

two complexes negated the stability difference. Therefore, nearly all NpO_2^+ was reduced to Np^{4+}, upholding the conclusions from extraction and spectrophotometry studies.

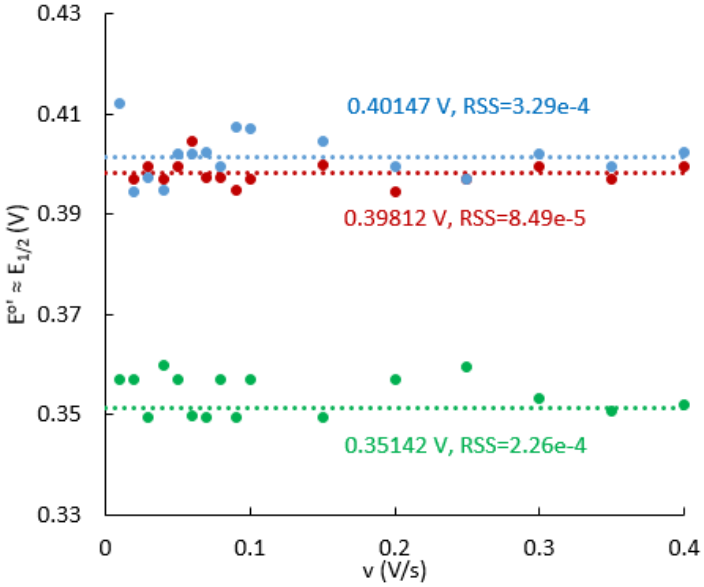

Figure 9. Dependence of the half-wave potential, $E_{1/2}$, and the formal potential, $E^{o'}$, of NpO_2^+ (magenta), HOPO (green), and Np-HOPO complex (blue) as a function of the scan rate from 0.01 V/s to 0.4 V/s, in 1 M HNO_3 solution.

Metal competition titrations. The extraordinarily high stability constant between M^{4+} and HOPO invalidates direct measurements, such as direct spectroscopic titrations [29], direct potentiometric titrations, NMR, or calorimetry [26]. Indirect probing techniques were thus sought here, including CV and spectrophotometric competition titrations. On the one hand, CV requires more than one stable oxidation state [26] and NpO_2^+ can be reduced by HOPO. On the other hand, it is hard to find a thermodynamically well-characterized ligand that is comparable with HOPO in the affinity to M^{4+} ions, so metal competition was adopted in this study.

UV-Vis spectra of HOPO, PuHOPO, and NpHOPO (**Figure S3**) show a $\pi \rightarrow \pi^*$ transition band centered at 323 nm, abiding by the feature of the positive correlation between ionic radius and peak wavelength observed in the study of Zr^{4+}, Hf^{4+}, and Sn^{4+} [26]. Upon gradual addition of Pu^{4+}, a slight red shift was observed from 323 nm to 324 nm, most likely because of the lesser acidity of Pu^{4+}, compared to Np^{4+}, which decreases the absorbance energy of the 1,2-HOPO chromophore moiety. An isosbestic point appeared at ~340 nm concomitantly. The interactions

between HOPO and Pu^{4+} or Np^{4+} are much stronger than the nitrate counterparts since the HOPO concentration was only 1/40000 (25 μM to 1 M) that of NO_3^-. The refined result yielded a proton independent cumulative formation constant, $\log\beta_{101}$, of 42.0 ± 0.6 for NpHOPO, marginally smaller than for PuHOPO with a reported value of $\log\beta_{101} = 43.5 \pm 0.7$ [29]. Similar measurements were also performed using Th^{4+} as the competitor for Np^{4+}. Unfortunately, the fit of collected titration spectra failed, despite changes observed in the region of interest (**Figure S4**).

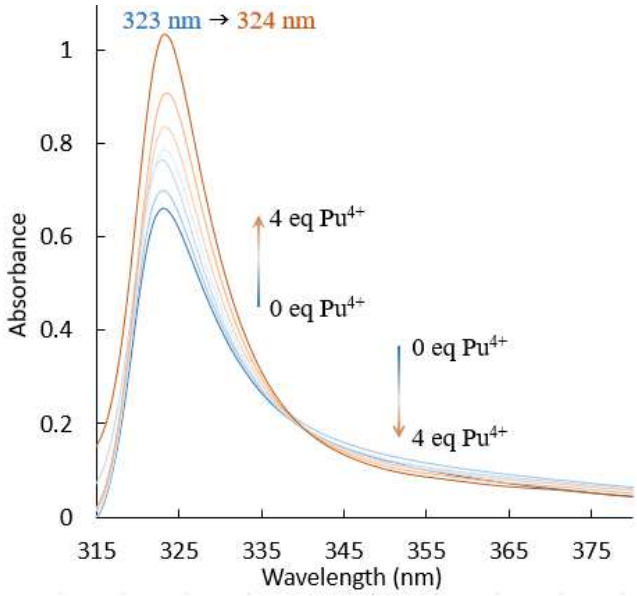

Figure 10. Metal competition spectrophotometric titration of NpHOPO against Pu^{4+}. [Np] = [HOPO] = 25 μM, Pu/Np = 0 – 4 mol/mol, [HNO_3] = 1 M, ambient temperature. Arrows indicate changes in absorbance as a result of Pu^{4+} addition.

The measured value for NpHOPO in this study is the first estimate of the formation constant of Np^{4+} complexed with HOPO, which advances the investigations of binding tetravalent metals with this chelator and suggests that the actinides might present a unique trend, different from the Th^{4+}-Ce^{4+}-Zr^{4+} trend published previously by our group [29].

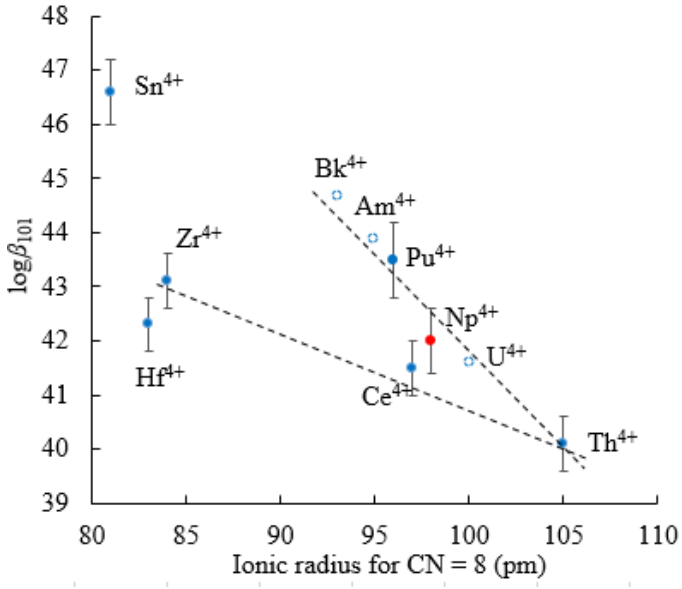

Figure 11. Cumulative formation constant for tetravalent metal-HOPO complexes as a function of metal ionic radii with a coordination number of 8. Values of blue solid points were taken from previously published results [23,25,26,29]; red solid point from this study; hollowed points from estimation based on the Th^{4+}-Np^{4+}-Pu^{4+} trend.

Conclusions

HOPO can reduce NpO_2^+ to Np^{4+} and bind Np^{4+}, as evidenced from the UV-Vis-NIR spectra and the CV studies. The cumulative stability constant of the corresponding NpHOPO complex was evaluated via the introduction of Pu^{4+} as a competitor. The reduction and stabilization by HOPO appeared very fast, which is opposed to what has been acknowledged thus far for the dioxo-bare metal transformation. This fast reaction rate makes centrifugal contactors a possible option in addition to the use of mixer-settlers and pulsed columns. The separation by liquid-liquid extraction among the actinide trio, UO_2^{2+}, NpO_2^+, and Pu^{4+}, was evaluated under very high acidities mimicking conditions of the PUREX process. Separations of Np from U and of Pu from U were both enhanced by the introduction of HOPO, due to the better valence and stability control offered by this ligand. As a result, a simplified version of PUREX was brought forward. The better valence control, stabilization of Np, and improved separation make HOPO a promising agent in the reprocessing of used nuclear fuel. Future work will continue elaborating upon these findings by evaluating the radiolytic stability of HOPO and by optimizing conditions for efficient separations.

Supporting Information

Supporting information is available free of charge, with additional experimental and calculated results.

Author Information

Corresponding Author

*E-mail: abergel@berkeley.edu.

Author Contributions

The manuscript was written through contributions of all authors. All authors have given approval to the final version of the manuscript.

ORCID

Yufei Wang: 0000-0002-5780-112X

Zhicheng Zhang: 0000-0002-2192-3846

Rebecca J. Abergel: 0000-0002-3906-8761

Acknowledgment

We thank Korey P. Carter for valuable discussions and Dr. Wayne Lukens for the $^{237}NpO_2^+$ in-house stock solution. This work was supported by the U.S. Department of Energy, Office of Science, Office of Basic Energy Sciences, Chemical Sciences, Geosciences, and Biosciences Division at the Lawrence Berkeley National Laboratory under Contract DE-AC02-05CH11231. We also acknowledge support from the DOE Office of Nuclear Energy's Nuclear Energy University Programs (DE-NE0008949) during manuscript assembly and submission.

Abbreviations

A/FHA, aceto-/formo-hydroxamic acid;

An, actinides;

CMPO, octyl(phenyl)-N,N-diisobutylcarbamoylmethylphosphine oxide;

CV, cyclic voltammetry;

HERL, Heavy Element Research Laboratory;

HDTPA, diethylenetriaminepentaacetic acid;

HEDTA, HydroxyEthyleneDiamineTetraAcetic acid, N-Hydroxyethyl-EthyleneDiamine-N, N', N'-TriAcetic acid;

HLLW, high level liquid waste;

HOPO, 3,4,3-LI(1,2-HOPO);

LBNL, Lawrence Berkeley National Laboratory;

PUREX, plutonium uranium redox extraction;

QR, quasi-reversible;

SPCarEs, screen-printed glassy carbon electrodes;

UNF, used nuclear fuel;

UREX, URanium Extraction.

References

(1) Yoshida, Z.; Johnson, S. G.; Kimura, T.; Krsul, J. R. Neptunium. In *The Chemistry of the Actinide and Transactinide Elements*; Morss, L. R., Edelstein, N. M., Fuger, J., Eds.; Springer Netherlands: Dordrecht, 2006; pp 699–812. https://doi.org/10.1007/1-4020-3598-5_6.

(2) Benedict, M.; Pigford, T. H. *Nuclear Chemical Engineering*; McGraw-Hill, 1957.

(3) Taylor, R. J.; Denniss, I. S.; Wallwork, A. L. Neptunium Control in an Advanced Purex Process. *Nuclear Energy* **1997**, *36* (1), 39–46.

(4) Modolo, G.; Geist, A.; Miguirditchian, M. 10 - Minor Actinide Separations in the Reprocessing of Spent Nuclear Fuels: Recent Advances in Europe. In *Reprocessing and Recycling of Spent Nuclear Fuel*; Taylor, R., Ed.; Woodhead Publishing Series in Energy; Woodhead Publishing: Oxford, 2015; pp 245–287. https://doi.org/10.1016/B978-1-78242-212-9.00010-1.

(5) Chen, H.; Taylor, R. J.; Jobson, M.; Woodhead, D. A.; Boxall, C.; Masters, A. J.; Edwards, S. Simulation of Neptunium Extraction in an Advanced PUREX Process—Model Improvement. *Solvent Extraction and Ion Exchange* **2017**, *35* (1), 1–18. https://doi.org/10.1080/07366299.2016.1273684.

(6) Nash, K. L.; Lumetta, G. J. *Advanced Separation Techniques for Nuclear Fuel Reprocessing and Radioactive Waste Treatment*; Elsevier, 2011.

(7) Simpson, M. F.; Law, J. D. Nuclear Fuel, Reprocessing Of. In *Nuclear Energy: Selected Entries from the Encyclopedia of Sustainability Science and Technology*; Tsoulfanidis, N., Ed.; Springer: New York, NY, 2013; pp 153–173. https://doi.org/10.1007/978-1-4614-5716-9_5.

(8) Bugrov, Konstantine. V.; Korotaev, V. G.; Korchenkin, K. K.; Logunov, M. V.; Lukin, S. A.; Mashkin, A. N.; Melentev, A. B.; Samarina, N. S. The Development and Testing of the New Flowsheets for the Plutonium Purification Cycle of the Purex Process. *Procedia Chemistry* **2016**, *21*, 162–166. https://doi.org/10.1016/j.proche.2016.10.023.

(9) Taylor, R. *Reprocessing and Recycling of Spent Nuclear Fuel*; Elsevier, 2015.

(10) Mahanty, B.; Kanekar, A. S.; Ansari, S. A.; Bhattacharyya, A.; Mohapatra, P. K. Separation of Neptunium from Actinides by Monoamides: A Solvent Extraction Study. *Radiochimica Acta* **2019**, *107* (5), 369–376. https://doi.org/10.1515/ract-2018-3074.

(11) Fox, O. D.; Jones, C. J.; Birkett, J. E.; Carrott, M. J.; Crooks, G.; Maher, C. J.; Roube, C. V.; Taylor, R. J. Advanced PUREX Flowsheets for Future Np and Pu Fuel Cycle Demands. In *Separations for the*

Nuclear Fuel Cycle in the 21st Century; ACS Symposium Series; American Chemical Society, 2006; Vol. 933, pp 89–102. https://doi.org/10.1021/bk-2006-0933.ch006.

(12) Chung, D.-Y.; Lee, E.-H. The Reduction of Np(VI) by Acetohydroxamic Acid in Nitric Acid Solution. *Bulletin of the Korean Chemical Society* **2005**, *26* (11), 1692–1694. https://doi.org/10.5012/bkcs.2005.26.11.1692.

(13) Brown, M. A.; Paulenova, A.; Gelis, A. V. Aqueous Complexation of Thorium(IV), Uranium(IV), Neptunium(IV), Plutonium(III/IV), and Cerium(III/IV) with DTPA. *Inorg. Chem.* **2012**, *51* (14), 7741–7748. https://doi.org/10.1021/ic300757k.

(14) Reed, D. T.; Wygmans, D. G.; Aase, S. B.; Banaszak, J. E. Reduction of Np(VI) and Pu(VI) by Organic Chelating Agents. *Radiochimica Acta* **1998**, *82* (s1), 109–114. https://doi.org/10.1524/ract.1998.82.special-issue.109.

(15) Deblonde, G. J.-P.; Sturzbecher-Hoehne, M.; Rupert, P. B.; An, D. D.; Illy, M.-C.; Ralston, C. Y.; Brabec, J.; de Jong, W. A.; Strong, R. K.; Abergel, R. J. Chelation and Stabilization of Berkelium in Oxidation State +IV. *Nature Chemistry* **2017**, *9* (9), 843–849. https://doi.org/10.1038/nchem.2759.

(16) Deblonde, G. J.-P.; Ricano, A.; Abergel, R. J. Ultra-Selective Ligand-Driven Separation of Strategic Actinides. *Nature Communications* **2019**, *10* (1). https://doi.org/10.1038/s41467-019-10240-x.

(17) KIHARA, T.; FUJINE, S.; FUKASAWA, T.; MATSUI, T.; MAEDA, M.; IKEDA, T. Laser Induced Photoacoustic Spectroscopy for Analysis of Neptunium(V) Ions under PUREX Process Condition. *Journal of Nuclear Science and Technology* **1996**, *33* (5), 409–413. https://doi.org/10.1080/18811248.1996.9731926.

(18) Niese, U.; Vecernik, J. Cyclic Voltammetry of Neptunium in Different Media. *Isotopenpraxis Isotopes in Environmental and Health Studies* **1982**, *18* (5), 191–192. https://doi.org/10.1080/10256018208544731.

(19) Ikeda-Ohno, A.; Hennig, C.; Rossberg, A.; Funke, H.; Scheinost, A. C.; Bernhard, G.; Yaita, T. Electrochemical and Complexation Behavior of Neptunium in Aqueous Perchlorate and Nitrate Solutions. *Inorg. Chem.* **2008**, *47* (18), 8294–8305. https://doi.org/10.1021/ic8009095.

(20) Yamamura, T.; Watanabe, N.; Yano, T.; Shiokawa, Y. Electron-Transfer Kinetics of Np[Sup 3+]/Np[Sup 4+], NpO[Sub 2][Sup +]/NpO[Sub 2][Sup 2+], V[Sup 2+]/V[Sup 3+], and VO[Sup 2+]/VO[Sub 2][Sup +] at Carbon Electrodes. *Journal of The Electrochemical Society* **2005**, *152* (4), A830. https://doi.org/10.1149/1.1870794.

(21) Carter, K. P.; Smith, K. F.; Tratnjek, T.; Shield, K. M.; Moreau, L. M.; Rees, J. A.; Booth, C. H.; Abergel, R. J. Spontaneous Chelation-Driven Reduction of the Neptunyl Cation in Aqueous Solution. *Chemistry – A European Journal* **2020**, *26* (11), 2354–2359. https://doi.org/10.1002/chem.201905695.

(22) Casadio, S.; Orlandini, F. Cyclic Voltammetry of Pu and Np in Nitric Acid Media. *Journal of Electroanalytical Chemistry and Interfacial Electrochemistry* **1971**, *33* (1), 212–215. https://doi.org/10.1016/S0022-0728(71)80224-3.

(23) Deblonde, G. J.-P.; Sturzbecher-Hoehne, M.; Abergel, R. J. Solution Thermodynamic Stability of Complexes Formed with the Octadentate Hydroxypyridinonate Ligand 3,4,3-LI(1,2-HOPO): A Critical Feature for Efficient Chelation of Lanthanide(IV) and Actinide(IV) Ions. *Inorganic Chemistry* **2013**, *52* (15), 8805–8811. https://doi.org/10.1021/ic4010246.

(24) Sturzbecher-Hoehne, M.; Choi, T. A.; Abergel, R. J. Hydroxypyridinonate Complex Stability of Group (IV) Metals and Tetravalent f-Block Elements: The Key to the next Generation of Chelating Agents for Radiopharmaceuticals. *Inorganic Chemistry* **2015**, *54* (7), 3462–3468. https://doi.org/10.1021/acs.inorgchem.5b00033.

(25) Deblonde, G. J.-P.; Lohrey, T. D.; An, D. D.; Abergel, R. J. Toxic Heavy Metal – Pb, Cd, Sn – Complexation by the Octadentate Hydroxypyridinonate Ligand Archetype 3,4,3-LI(1,2-HOPO). *New Journal of Chemistry* **2018**, *42* (10), 7649–7658. https://doi.org/10.1039/C7NJ04559J.
(26) Deblonde, G. J.-P.; Lohrey, T. D.; Abergel, R. J. Inducing Selectivity and Chirality in Group IV Metal Coordination with High-Denticity Hydroxypyridinones. *Dalton Transactions* **2019**, *48* (23), 8238–8247. https://doi.org/10.1039/C9DT01031A.
(27) Sturzbecher-Hoehne, M.; Ng Pak Leung, C.; D'Aléo, A.; Kullgren, B.; Prigent, A.-L.; Shuh, D. K.; Raymond, K. N.; Abergel, R. J. 3,4,3-LI(1,2-HOPO): In Vitro Formation of Highly Stable Lanthanide Complexes Translates into Efficacious in Vivo Europium Decorporation. *Dalton Transactions* **2011**, *40* (33), 8340. https://doi.org/10.1039/c1dt10840a.
(28) Gans, P.; Sabatini, A.; Vacca, A. Investigation of Equilibria in Solution. Determination of Equilibrium Constants with the HYPERQUAD Suite of Programs. *Talanta-Oxford* **1996**, *43* (10), 1739–1754.
(29) Sturzbecher-Hoehne, M.; Choi, T. A.; Abergel, R. J. Hydroxypyridinonate Complex Stability of Group (IV) Metals and Tetravalent f-Block Elements: The Key to the Next Generation of Chelating Agents for Radiopharmaceuticals. *Inorganic Chemistry* **2015**, *54* (7), 3462–3468. https://doi.org/10.1021/acs.inorgchem.5b00033.
(30) Wang, Y.; Deblonde, G. J.-P.; Abergel, R. J. Hydroxypyridinone Derivatives: A Low-PH Alternative to Polyaminocarboxylates for TALSPEAK-like Separation of Trivalent Actinides from Lanthanides. *ACS Omega* **2020**. https://doi.org/10.1021/acsomega.0c00873.
(31) Lahr, H.; Knoch, W. *Determination of Stability Constants of Some Actinide Complexes. II. Nitrate and Chloride Complexes of Uranium, Neptunium, Plutonium and Americium*; 1970.
(32) P. Carter, K.; Jian, J.; M. Pyrch, M.; Z. Forbes, T.; M. Eaton, T.; J. Abergel, R.; Jong, W. A. de; K. Gibson, J. Reductive Activation of Neptunyl and Plutonyl Oxo Species with a Hydroxypyridinone Chelating Ligand. *Chemical Communications* **2018**, *54* (76), 10698–10701. https://doi.org/10.1039/C8CC05626A.
(33) Edelstein, N. M.; Fuger, J.; Morss, L. R. *The Chemistry of the Actinide and Transactinide Elements*; Springer, 2006.
(34) Bard, A. J.; Faulkner, L. R. Fundamentals and Applications. *Electrochemical Methods* **2001**, *2* (482), 580–632.
(35) Elgrishi, N.; Rountree, K. J.; McCarthy, B. D.; Rountree, E. S.; Eisenhart, T. T.; Dempsey, J. L. A Practical Beginner's Guide to Cyclic Voltammetry. *Journal of Chemical Education* **2018**, *95* (2), 197–206. https://doi.org/10.1021/acs.jchemed.7b00361.
(36) Nicholson, R. S. Theory and Application of Cyclic Voltammetry for Measurement of Electrode Reaction Kinetics. *Analytical Chemistry* **1965**, *37* (11), 1351–1355. https://doi.org/10.1021/ac60230a016.